Diagnosis of Variability and Trends in a Global Precipitation Dataset Using a Physically Motivated Statistical Model

M. R. P. SAPIANO

Department of Meteorology, University of Reading, Reading, United Kingdom, and Earth Systems Science Interdisciplinary Center, University of Maryland, College Park, College Park, Maryland

D. B. STEPHENSON

Department of Meteorology, University of Reading, Reading, United Kingdom

H. J. GRUBB

School of Applied Statistics, University of Reading, Reading, United Kingdom

P. A. ARKIN

Earth Systems Science Interdisciplinary Center, University of Maryland, College Park, College Park, Maryland

(Manuscript received 5 May 2005, in final form 16 December 2005)

ABSTRACT

A physically motivated statistical model is used to diagnose variability and trends in wintertime (October–March) Global Precipitation Climatology Project (GPCP) pentad (5-day mean) precipitation. Quasi-geostrophic theory suggests that extratropical precipitation amounts should depend multiplicatively on the pressure gradient, saturation specific humidity, and the meridional temperature gradient. This physical insight has been used to guide the development of a suitable statistical model for precipitation using a mixture of generalized linear models: a logistic model for the binary occurrence of precipitation and a Gamma distribution model for the wet day precipitation amount.

The statistical model allows for the investigation of the role of each factor in determining variations and long-term trends. Saturation specific humidity q_s has a generally negative effect on global precipitation occurrence and with the tropical wet pentad precipitation amount, but has a positive relationship with the pentad precipitation amount at mid- and high latitudes. The North Atlantic Oscillation, a proxy for the meridional temperature gradient, is also found to have a statistically significant positive effect on precipitation over much of the Atlantic region. Residual time trends in wet pentad precipitation are extremely sensitive to the choice of the wet pentad threshold because of increasing trends in low-amplitude precipitation pentads; too low a choice of threshold can lead to a spurious decreasing trend in wet pentad precipitation amounts. However, for not too small thresholds, it is found that the meridional temperature gradient is an important factor for explaining part of the long-term trend in Atlantic precipitation.

1. Introduction

Precipitation is an important weather element whose future changes will have a large impact on society (e.g., more droughts and floods). Recent flooding events in the United Kingdom such as those in October and November 2000 [Department for Environment, Food, and Rural Affairs (DEFRA) 2001], November 2002, and January 2003 have brought this problem to the forefront of the public mind and have lead to substantial insurance losses (Hawes 2003).

The Intergovernmental Panel on Climate Change (IPCC) concluded that global average surface temperature had increased by 0.6° ± 0.2°C over the twentieth century (Houghton et al. 2001) and that there is evidence that most of the warming observed over the last 50 yr is attributable to human activities. However, there

Correspondening author address: M. R. P. Sapiano, ESSIC, Computer and Space Sciences Building, University of Maryland, College Park, College Park, MD 20740.
E-mail: msapiano@essic.umd.edu

is less certainty associated with trends in precipitation. Houghton et al. (2001) concluded that precipitation amounts have increased over much of the globe, with a decrease over subtropical areas, but that the detection of these trends is problematic because they are neither temporally nor spatially uniform (Folland et al. 2001). Furthermore, the underlying cause of trends in regional precipitation remains unclear.

Global gauge/satellite precipitation datasets are available from 1979, but a careful subseasonal statistical analysis of such datasets has yet to be published in the mainstream literature. The main aim of this study is explore the dominant causes of variability in extratropical precipitation and investigate the effect of these factors on global precipitation trends.

Precipitation is highly discontinuous and occurs only during wet events that have nonuniform duration, frequency, and intensity. These events aggregate to form the daily and monthly rainfall totals routinely measured at individual stations and much of the work on trends in precipitation has concentrated on the analysis of seasonal mean precipitation since this has a more Gaussian (normal) distribution that is amenable to simple analysis techniques. However, seasonal mean precipitation is far removed from the subdaily time scales of the underlying processes.

A common failing of statistical studies is to select the model based only on the available data. A major aim of this study has been to use physical insight to inform the choice of the statistical model as well as the explanatory variables. Therefore, we present a physically motivated probability model for pentad (5-day mean) precipitation across the globe. The physical motivation is also used to identify the most important factors for explaining precipitation variations. The statistical model can then be used to study how these factors help account for the long-term time trends in precipitation.

This article is structured as follows. Section 2a uses quasigeostrophic theory to identify the key factors affecting extratropical large-scale winter precipitation. The main factors are local sea level pressure (SLP), saturation specific humidity q_s, and the meridional temperature gradient. The physical motivation is then used to develop a suitable statistical model in section 2b. The chosen method models the probability of the occurrence of precipitation with a Bernoulli distribution and then separately models the wet pentad precipitation amount with a Gamma distribution. The Bernoulli and Gamma distributions are allowed to depend on explanatory factors using an extended regression approach known as generalized linear modeling (GLM; Nelder and Wedderburn 1972). The model fitting is described in section 2c. The pentad data is described in section 3. Section 4 then applies the mixture GLM to precipitation at each gridpoint of October–March winter pentad Global Precipitation Climatology Precipitation (GPCP). Sea level pressure and saturation specific humidity are used as explanatory factors as is the North Atlantic Oscillation, which is used as a proxy for the meridional temperature gradient.

2. A physically motivated statistical model for diagnosis of precipitation

a. Physical considerations

The time-averaged vertically averaged water budget can be written as

$$\int_{p_c}^{p_t} \nabla \cdot (\overline{q\mathbf{v}})\, dp + [\overline{\omega q_s}]_{p_c}^{p_t} = \overline{e} - \overline{c},$$

where q is specific humidity, $\mathbf{v}$ is the horizontal component of vector velocity, p is pressure, ω is vertical velocity in pressure coordinates, e and c represent atmospheric evaporation and condensation, respectively, and p_c and p_t represent pressure at the condensation level and the top of the troposphere, respectively (Peixoto and Oort 1992).

The horizontal divergence term is generally small in comparison to the other terms. Since evaporation is generally small above the condensation level, the right-hand side is approximately the rate of precipitation. Assuming that the air is fully saturated above the condensation level, the precipitation rate can be approximated by $\overline{q_s\omega}$, where q_s is the saturation specific humidity. This can be expressed in SI units of m s^{-1} by multiplying this by the density of air, ρ_a, and dividing by the density of water, ρ_w and using vertical velocity, w, in m s^{-1} as

$$\frac{\rho_a \overline{q_s w}}{\rho_w} \quad w > 0. \tag{1}$$

This expression can be used to obtain a rough estimate of the precipitation rate during the passage of an extratropical cyclone. Typical extratropical cyclone values of $\rho_w \sim 10^3$ kg m^{-3}, $\rho_a \sim 1$ kg m^{-3}, $\overline{q}_s \sim 10^{-2}$ kg kg^{-1}, and $w \sim 10^{-2}$ m s^{-1} close to the surface give a precipitation rate of $\sim 10^{-7}$ m s^{-1}, equivalent to a value of 10 mm day^{-1} that is typically observed.

Saturation specific humidity q_s is given by $q_s = \varepsilon e_s/p$, where $\varepsilon = 0.6213$ is the ratio of the molar masses of dry air and water vapor, and p is pressure, and e_s is saturation vapor pressure. The saturation vapor pressure e_s is exponentially related to temperature by the Clausius–Clapeyron equation (Rogers and Yau 1989). Previous studies have demonstrated that there is a significant positive correlation between monthly mean precipitation and temperature in the wintertime extratropics (Madden and Williams 1978; Trenberth and Shea 2005). Precipitation amounts are limited by the water-holding capacity (the saturation humidity) and warm air advection in cyclonic storms (Sapiano 2004; Trenberth and Shea 2005).

Quasigeostrophic theory can be used in the extratropics to estimate the vertical velocity, ω, in terms of the geostrophic wind. This diagnostic equation is known as the *omega equation* (Hoskins et al. 1978; Durran and Snellman 1987). The terms representing the horizontal advection of vorticity and thermal advection in the omega equation are often of similar magnitude, opposite sign, and often cancel each other out (Hoskins et al. 1978; Trenberth 1978). Hoskins et al. (1978) introduced the Q-vector approach, where the Q vector is equal to the rate of change of the horizontal potential temperature gradient, which would develop in a fluid parcel moving with the geostrophic wind if the vertical velocity was exactly zero (Durran and Snellman 1987).

The omega equation can be written in Q-vector form as

$$\left(\sigma\boldsymbol{\nabla}_h^2 + f^2\frac{\partial^2}{\partial p^2}\right)\omega = -2\boldsymbol{\nabla}\cdot\mathbf{Q}, \tag{2}$$

where f is the Coriolis parameter, σ is the static stability, which is a function of the basic state temperature in the midtroposphere, and $\mathbf{Q}$ is the two-dimensional Q vector given by

$$\mathbf{Q} = \left[\frac{\partial\mathbf{v}_g}{\partial x}\cdot\boldsymbol{\nabla}\left(\frac{\partial\Phi}{\partial p}\right), \frac{\partial\mathbf{v}_g}{\partial y}\cdot\boldsymbol{\nabla}\left(\frac{\partial\Phi}{\partial p}\right)\right]. \tag{3}$$

Convergent $\mathbf{Q}$ is associated with ascent, whereas divergent $\mathbf{Q}$ is associated with subsidence (Hoskins and Pedder 1980). Sanders and Hoskins (1990) showed that (3) can be rewritten more simply as

$$\mathbf{Q} = -\frac{R}{P}\frac{\partial T}{\partial y}\boldsymbol{\nabla}\upsilon_g, \tag{4}$$

where υ_g is the meridional geostrophic wind component and $\partial T/\partial y$ is the meridional temperature gradient in the midtroposphere (e.g., at 500 hPa). Rewriting in terms of time mean and transient components gives

$$\mathbf{Q} = -\frac{R}{P}\frac{\partial\overline{T}}{\partial y}\boldsymbol{\nabla}\overline{\upsilon}_g - \frac{R}{P}\frac{\partial\overline{T}}{\partial y}\boldsymbol{\nabla}\upsilon_g' - \frac{R}{P}\frac{\partial T'}{\partial y}\boldsymbol{\nabla}\overline{\upsilon}_g - \frac{R}{P}\frac{\partial T'}{\partial y}\boldsymbol{\nabla}\upsilon_g'. \tag{5}$$

It is reasonable in midlatitudes to assume that $\overline{\upsilon}_g \ll \upsilon_g'$ and $(\partial T'/\partial y) \ll (\partial\overline{T}/\partial y)$ and so

$$\mathbf{Q} \approx -\frac{R}{P}\frac{\partial\overline{T}}{\partial y}\boldsymbol{\nabla}\upsilon_g'; \tag{6}$$

therefore,

$$\omega \approx \left(\sigma\nabla^2 + f^2\frac{\partial^2}{\partial p^2}\right)^{-1}\left(\frac{2R}{f\rho p}\frac{\partial\overline{T}}{\partial y}\nabla^2\frac{\partial p'}{\partial x}\right). \tag{7}$$

Equation (7) shows that ω is a function of the transient pressure anomaly p', the time-mean meridional temperature gradient $(\partial\overline{T}/\partial y)$ and the static stability σ. Hence, a stronger meridional temperature gradient will increase vertical velocities for a given pressure anomaly p'. Static stability has an inverse effect on vertical motion: reduction in static stability will enhance vertical velocities. Note that static stability is also a possible factor, but previous studies suggest that this is unlikely to change substantially beyond natural variability (Pavan et al. 1999). Equations (1) and (7) suggest that precipitation is the product of saturation specific humidity, the pressure anomaly, and the meridional temperature gradient.

The dry quasigeostrophic equations neglect certain terms contained in the primitive equations, such as enhanced vertical motion due to diabatic processes (the release of latent heat) and frictional effects. Räisänen (1995) compared the quasigeostrophic omega equation with a hydrostatic generalized omega equation and found a correlation of 0.7 between the ω estimated using the quasigeostrophic and generalized omega equations in midlatitudes. Räisänen (1995) concluded that, while the dominant causes of vertical motion in the midlatitudes are vorticity and thermal advection, the effect from diabatic heating is far from negligible. Therefore, the quasigeostrophic omega equation provides a good first-order approximation for estimating synoptic-scale vertical velocities, but a more detailed treatment that includes diabatic effects may be required for smaller-scale effects such as those that dominate in the warm season. Note also that the quasigeostrophic approximation only applies in the extratropics, and that factors affecting tropical precipitation might be different to those in the extratropical cold season.

b. A statistical model for precipitation

Coe and Stern (1982) suggested a two-component mixture model for modeling the occurrence of precipitation and the precipitation amount on a wet day. Binary precipitation occurrence, $W = 0$ or 1, was modeled as a Bernoulli distribution $P(W = w) = \pi^w(1-\pi)^{(1-w)}$. Wet days were defined as days on which the precipitation amount exceeded a small threshold y_0. The precipitation amount on a wet day was modeled using a Gamma distribution with mean μ and constant shape parameter ν. The parameters π and μ can be made to depend on explanatory variables $x_1, x_2, \ldots, x_p$. This model provides a method for exploring the effect of the identified factors on precipitation, and is multiplicative due to the log link. This type of model has been used in several previous studies (Stern and Coe 1984; Buishand and Tank 1996; Brandsma and Buishand 1997; Buishand and Brandsma 1999; Chandler and Wheater 2002), but not for investigating trends and variations in global precipitation datasets.

The binary response variable W is Bernoulli distributed with a *log odds* (i.e., the log of the probability of an event, divided by the probability that it does not occur) that depends on a linear combination of explanatory variables. The occurrence of precipitation W is modeled using a *logistic* regression given by

$$W|\eta \sim \mathrm{Be}(\pi)$$
$$\log\left(\frac{\pi}{1-\pi}\right) = \eta = \lambda_0 + \lambda_1 x_1 + \ldots + \lambda_j x_j + \ldots + \lambda_p x_p, \tag{8}$$

where $W = 1$ on a wet day and $W = 0$ otherwise. The nonlinear link function $\log[\pi/(1-\pi)]$ is linearly related to the p explanatory variables with $p + 1$ intercept and slope parameters, λ_j ($j = 0, \ldots, p$).

One of the main problems of GLMs is that the model parameters are not generally on the same scale as the response due to the nonlinear link function {e.g., $g(\pi) = \log[\pi/(1-\pi)]$ in Eq. (8)}. The parameters can be presented informatively by showing the change in the response due to a unit increase in the explanatory variable. For example, the odds $\pi/(1-\pi)$ is given by $\exp(\lambda_0 + \lambda_1 x_1 + \ldots + \lambda_p x_p)$ and so a unit change in x_1 will cause the odds to change by a factor of e^{λ_1}. Hence, $(e^{\lambda_1} - 1) \times 100$ gives the percentage change in the odds of precipitation for a unit change in x_1.

The wet day precipitation amount Y_w is modeled using a Gamma distribution as follows:

$$Y_w|\eta \sim \mathrm{Gamma}(\mu,\nu)$$
$$\log(\mu) = \eta = \kappa_0 + \kappa_1 x_1 + \ldots + \kappa_j x_j + \ldots + \kappa_p x_p$$
$$\nu = \text{constant}, \tag{9}$$

where Gamma (.) represents the Gamma distribution. The log of the mean wet day precipitation, $\log(\mu)$, is linearly related to the p explanatory variables by $p + 1$ parameters, κ_j ($j = 0, \ldots, p$). See Nelder and Wedderburn (1972) for further discussion of this GLM. By using a logarithmic link, the factors affecting the wet day mean precipitation amount become multiplicative as suggested by the physical arguments presented earlier. The assumption of constant shape ν implies a constant coefficient of variation (the ratio of the mean and the standard deviation) for fixed values of $x_1, \ldots, x_p$.

Because of the logarithmic link function, the parameters are not on the same scale as the response. The parameters can be expressed in terms of the unit change in response to a unit change in any of the explanatory variables. For example, the percentage unit change in μ due to a unit change in x_1 is given by $(e^{\kappa_1} - 1) \times 100$.

c. *Estimation of the model parameters*

The mixture model has been fitted to global gridded estimates of October–March precipitation. At each grid point, the parameters of the mixture model were estimated independently of the other grid points. Since an extended winter is to be used, sine and cosine explanatory variables in calendar day were also included in the models to account for the fixed annual cycle. All explanatory variables have been fitted as anomalies to their long-term mean so that the intercept represents the mean wet pentad odds for the occurrence model and the mean wet pentad precipitation amount in the wet pentad precipitation model, both of which will be taken for the year 2003. A long-term residual time trend is included by also adding the year as an explanatory variable in the model. All parameters are assumed to be stationary in time, although nonstationarity could be examined by the inclusion of interaction terms. Such interaction terms have not been included here, since this would lead to a much more complex model.

An advantage of a parametric model–based statistical approach is that it allows the statistical significance of the parameters in the model to be rigorously tested. Although for brevity the statistical significance of the parameters will not be shown here, only relationships that are at least statistically significant at the 5% level will be discussed.

The study of precipitation using the mixture GLM requires the selection of a wet pentad threshold. Since precipitation magnitude varies considerably across the globe, a spatially variable threshold is desirable. The threshold has been defined here using the 25th percentile of the wet pentad distribution at each grid point. This is later compared with a globally uniform threshold of 0.1 mm day^{-1}. The higher 25th percentile threshold is required to eliminate the effect of spurious trends in light precipitation.

3. Data

a. *The response variable: Precipitation*

The GPCP pentad precipitation dataset is a merged satellite/gauge estimate of global precipitation on a grid with 2.5° by 2.5° spatial resolution (Xie et al. 2003). The dataset used here covers the period 1979–2001. Since

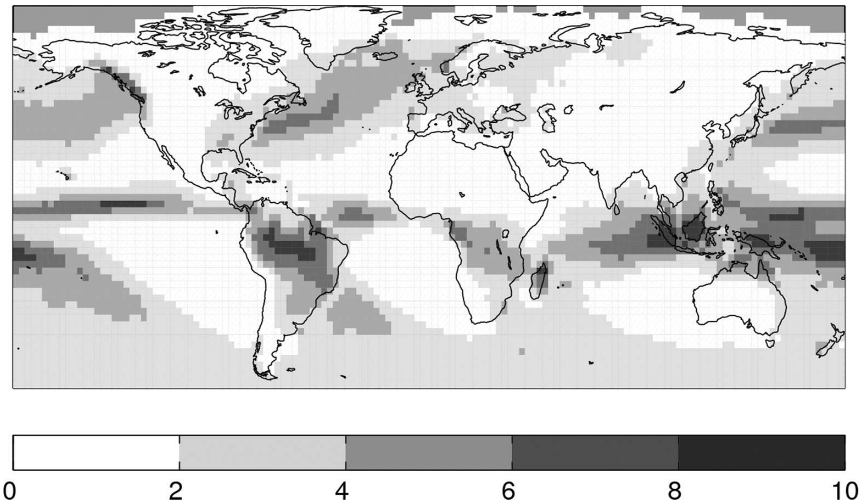

FIG. 1. Long-term mean of October–March winter GPCP pentad precipitation for the period 1979–2001. Units: mm day^{-1}.

the available satellite data covers a relatively short time period, an extended October–March winter analysis has been used in order to increase the sample size to 792 pentads. Similar results are obtained using a shorter December–February (DJF) winter season (not shown), but the resulting fields are noisier. The GPCP global precipitation dataset (which will be referred to as simply GPCP) is used as the primary dataset for global analysis, since it is the longest global record with pentad temporal resolution.

Figure 1 shows the mean pentad precipitation for October–March winters from 1979 to 2001. The maximum precipitation occurs around the tropical convergence zones. Noteworthy features include the intertropical convergence zone (ITCZ) just north of the equator, the precipitation maxima over northern parts of South America and Central Africa, the arid desert regions of North Africa and southern Asia, and the dry subtropical regions of ascent over the oceans in the Southern Hemisphere. In midlatitudes, precipitation is dominated by extratropical cyclones and is maximum in storm tracks over the Atlantic and Pacific Oceans. Precipitation in high latitudes is generally low.

b. The explanatory variables: Pressure, saturation specific humidity, and the temperature gradient

Sea level pressure, saturation specific humidity, and the meridional temperature gradient were identified as explanatory variables for the statistical modeling in section 2a.

1) SEA LEVEL PRESSURE

Equation (7) shows that pressure gradient dp'/dx is an important factor for vertical motion. Imagine a sinusoidal baroclinic wave such as that proposed by Eady (1949) where the upper-level wave is a quarter of a wavelength out of phase with the surface wave. Of interest in this study is the vertical velocity in the midtroposphere, which is collocated with the surface low due to the vertical phase tilt. Therefore, SLP is used in this analysis. Local sea level pressure series at each grid point have been obtained from the 40-year European Centre for Medium-Range Weather Forecasts (ECMWF) Re-Analysis (ERA-40; Simmons and Gibson 2000). The fine resolution ERA-40 analysis data was transferred to the coarser GPCP grid using linear interpolation.

2) SATURATION SPECIFIC HUMIDITY

Saturation specific humidity can be calculated from saturation vapor pressure. A simple method of calculating saturation vapor pressure from temperature and SLP was presented by Murray (1967). This method was used here to combine SLP and 2-m temperature data obtained from the ERA-40 reanalysis to yield global gridded values of derived q_s. Figure 2 shows the linear time trend in October–March winter mean q_s over the period 1979–2001. The trends in q_s closely follow trends in temperature. Folland et al. (2001) showed the mean DJF temperature trends over the globe from 1976 to 2001. The main features of Fig. 2 are similar to those shown by Folland et al. (2001), with positive trends over Europe and much of the Atlantic, and a mix of positive and negative trends over the Pacific. However the large positive trend over central Asia reported by Folland et al. (2001) is not evident in saturated specific humidity, and the trend over the northwest of North America has the opposite sign to that in Folland et al. (2001). The large negative trend over much of the Pacific Ocean is

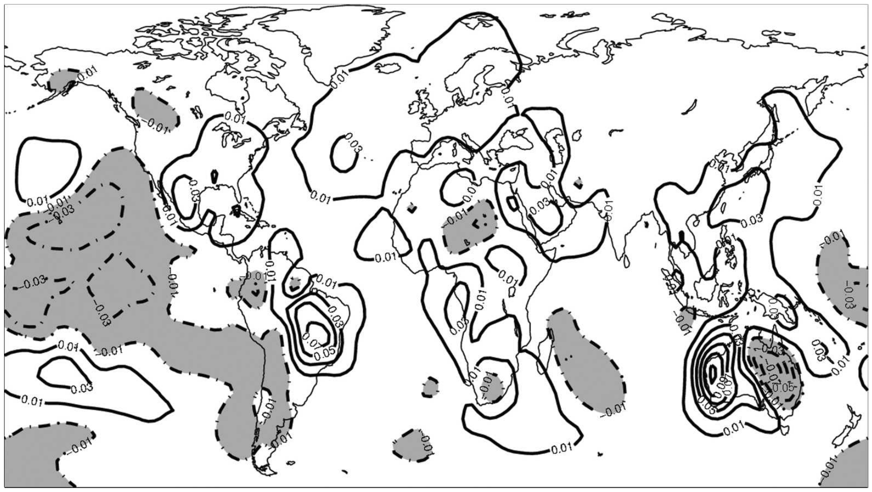

FIG. 2. Long-term linear time trend in October–March saturation specific humidity over the period 1979–2001. Units: g kg^{-1} yr^{-1}. The 1–2–1 smoothing applied for readability. Solid lines indicate positive contours starting at 0.01 g kg^{-1} with dashed lines and shading to indicate negative contours starting at -0.01 g kg^{-1}. The contour interval is 0.02 g kg^{-1} and the zero line has been omitted.

smaller and does not extend as far spatially in the analysis of Folland et al. (2001). Investigation of the ERA-40 DJF 2-m temperature trend (not shown) reveals that the differences in sign are mainly caused by the influence of October, November, and March in the extended boreal winter analysis, but that the lower magnitudes in the trends over Russia and the northwest of North America are possibly due to the different time period used by Folland et al. (2001).

3) Meridional temperature gradient

Away from the equator, the meridional temperature gradient (MTG) in Eq. (4) is related to the vertical shear in the zonal wind by the thermal wind relation:

$$\frac{\partial \overline{u}_g}{\partial p} = \frac{R}{fp}\frac{\partial \overline{T}}{\partial y}, \tag{10}$$

where u_g is the geostrophic zonal wind and p is the vertical pressure coordinate. The strongest zonal wind shear occurs in regions with the strongest meridional temperature gradients. By geostrophy, the zonal wind is in turn related to the meridional gradient in geopotential height as follows:

$$\overline{u}_g = -\frac{g}{f}\frac{\partial \overline{Z}}{\partial y}, \tag{11}$$

where Z is geopotential height. Hence, the meridional gradient in geopotential height (or sea level pressure) as estimated by the North Atlantic Oscillation (NAO) index provides a measure of the strength of the zonal flow and hence the meridional temperature gradient over the North Atlantic and western Europe (Wanner et al. 2001; Stephenson et al. 2003). When NAO is strongly positive, the zonal flow in the North Atlantic is stronger than normal and there is a stronger meridional temperature gradient in the upper troposphere. Hence, from the omega equation, one should expect more precipitation for a given vertical velocity during periods when NAO is strongly positive. This dynamical effect of the NAO on precipitation is in addition to NAO's effect on northward steering of North Atlantic storms.

The link between the NAO and European precipitation is supported by several authors who have linked the north–south shift of the storm tracks to precipitation (Hurrell 1995; Türkeş and Erlat 2003; Uvo 2003; Trigo et al. 2004). However, Eq. (7) shows that the NAO is also related to increased *precipitation intensity* due to a strengthened MTG.

Jones et al. (2003) reviewed methods for monitoring the NAO. The simplest approach is to calculate the difference in mean SLP at points over Iceland and the Azores. A more robust approach is to take the first principal component (PC) time series of regional (or Northern Hemispheric) SLP. Barnston and Livezey (1987) calculated an NAO index based on a rotated principal components analysis of Northern Hemispheric 700-hPa geopotential height anomalies. This series will be used here as a proxy for the meridional temperature gradient. The daily Climate Prediction Center (CPC) series has been averaged here to make pentad means.

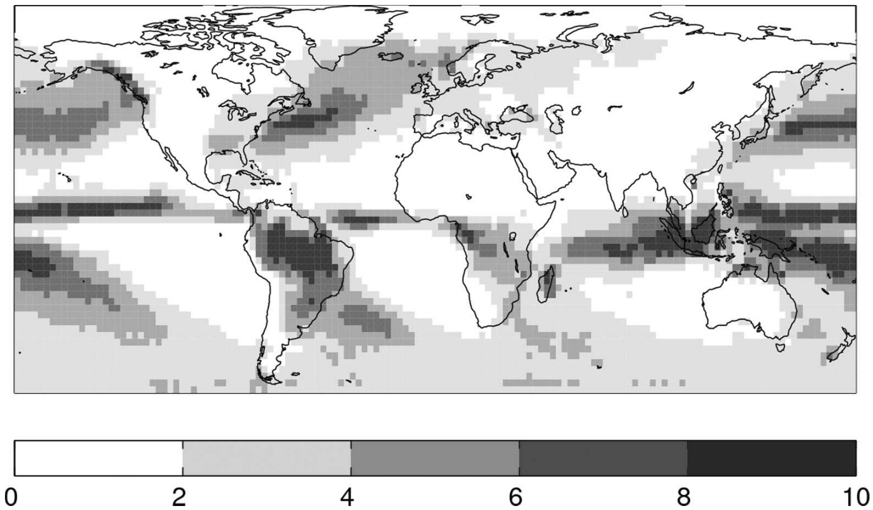

FIG. 3. Long-term mean of October–March winter GPCP wet pentad precipitation amount $e^{\hat{\kappa}_0}$ for the period 1979–2001. Units: mm day^{-1}.

4. Results

Figure 3 shows the estimated mean wet pentad precipitation amount $e^{\hat{\kappa}_0}$. As might be expected, the mean wet pentad precipitation has a similar global pattern to the mean precipitation shown in Fig. 1. Figure 3 highlights areas where the precipitation is particularly intense when it does occur, such as over the rain forests and in the Tropics. Figure 4 shows the estimated shape parameter $\hat{\nu}$ at each grid point. In general, areas with a high mean precipitation also have a large shape parameter. A Gamma distribution with a shape parameter greater than unity resembles the normal distribution with a slight positive skew. This behavior is seen over much of the globe in Fig. 4. A Gamma distribution with a shape parameter less than or equal to unity is monotonically decreasing (inverted J shape) and occurs in Fig. 4 in extremely dry areas such as the deserts, the subtropics, and the Southern Hemisphere oceanic subsidence regions.

a. Dependence on SLP

Figure 5a shows the SLP parameter estimate $(e^{\hat{\lambda}_1} - 1) \times 100\%$ across the globe. Since the variability of SLP is meridionally inhomogeneous, SLP has been standard-

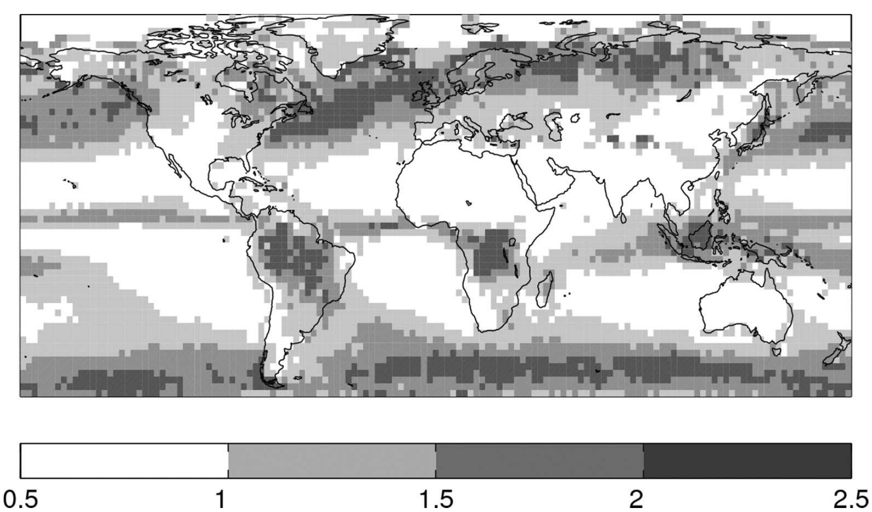

FIG. 4. Shape parameter estimates $\hat{\nu}$ for October–March wet pentad GPCP precipitation amount from the full model over the period 1979–2001 with the wet pentad threshold set to the 25th percentile.

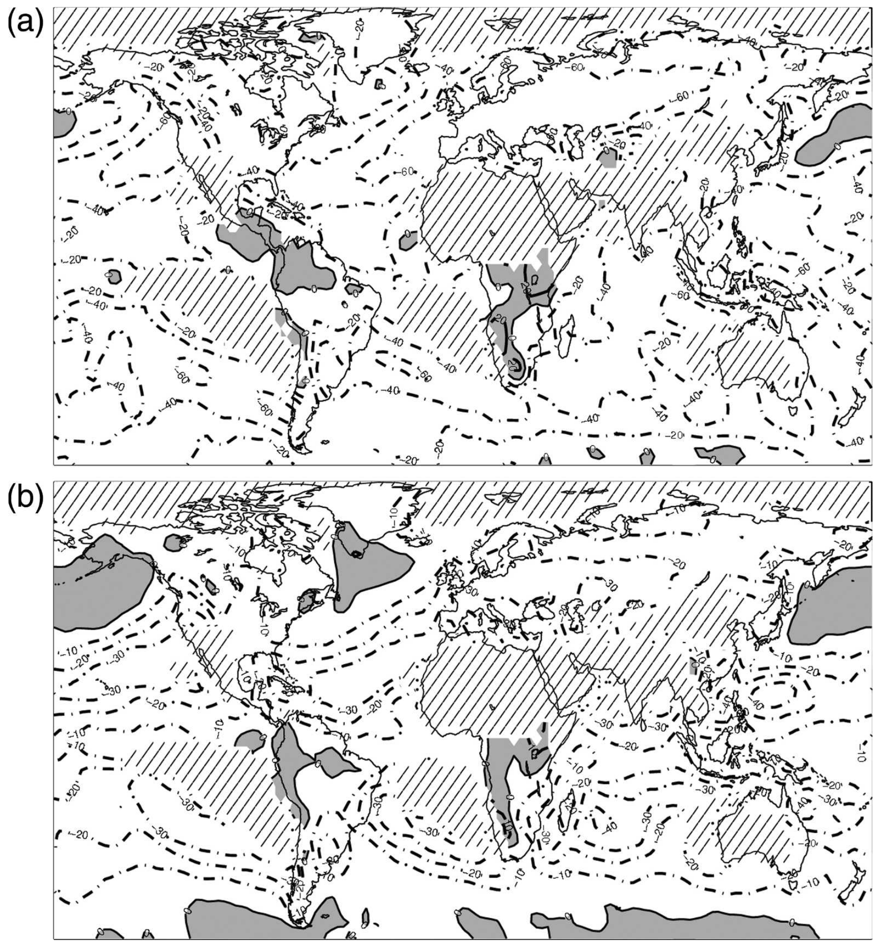

FIG. 5. Standardized SLP parameter estimates for October–March wet pentad GPCP precipitation (a) occurrence $(e^{\hat{\lambda}_1} - 1) \times 100\%$ and (b) amount $(e^{\hat{\kappa}_1} - 1) \times 100\%$ from the full model over the period 1979–2001 with the wet pentad threshold set to the 25th percentile. Units: %. The 1–2–1 smoothing applied for readability. Shading and solid lines indicate positive contours and dashed lines indicate negative contours. Contour interval is (a) 20% and (b) 10%. Hatching indicates areas where the model could not be fitted.

ized by its own standard deviation in the model. The standard deviation of sea level pressure is almost latitudinally homogeneous with the lowest values in the Tropics and the highest values toward the Poles. Exceptions to this pattern occur over large landmasses such as North America and northern Asia where the standard deviation is lower and at the end of the storm tracks where the standard deviation is considerably higher. This standardization allows for comparison of different areas of the globe, although the units become percentage change *per standard deviation*. Note that this does not have any effect on the sign or the statistical significance of the parameter, but can alter the magnitude. There is a strong negative relationship between the odds of precipitation occurring and SLP over nearly all of the globe. Notable exceptions appear over the Tropics where convection dominates and the relationship is weaker or even positive. The negative relationship can reach up to a 50% reduction in the odds of precipitation for a one standard deviation change in SLP. Figure 5b shows the SLP parameter estimates $(e^{\hat{\kappa}_1} - 1) \times 100\%$ for the wet pentad precipitation amount. As with the model for the precipitation occurrence, the relationship between the wet pentad precipitation and SLP is negative over much of the globe. There is a weaker relationship between SLP and precipitation amount over the Tropics. However, there is a small intriguing positive relationship on the poleward side of the storm tracks.

b. Dependence on saturation specific humidity

Figure 6a shows the q_s parameter estimates $(e^{\hat{\lambda}_2} - 1) \times 100\%$ for precipitation occurrence. The relationship is

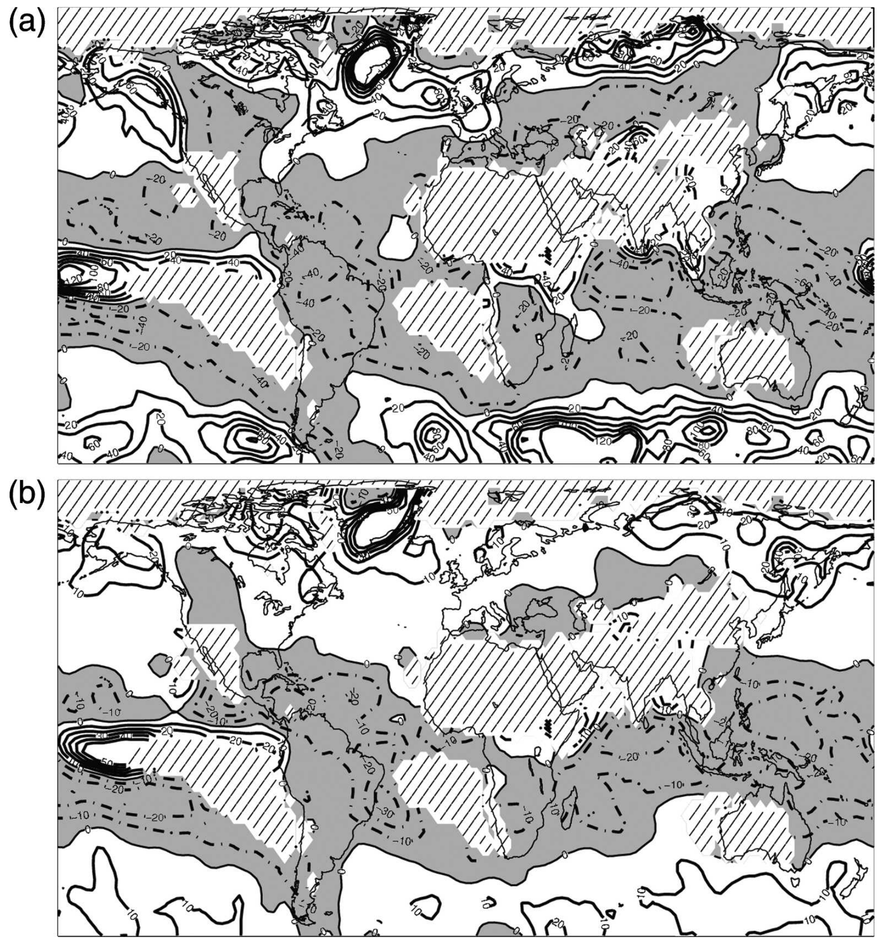

FIG. 6. Saturation specific humidity q_s parameter estimates for October–March wet pentad GPCP precipitation (a) occurrence $(e^{\hat{\lambda}_2} - 1) \times 100\%$ and (b) amount $(e^{\hat{\kappa}_2} - 1) \times 100\%$ from the full model over the period 1979–2001 with the wet pentad threshold set to the 25th percentile. Units: % $(\mathrm{g\ kg}^{-1})^{-1}$. The 1–2-1 smoothing is applied for readability. Solid lines indicate positive contours with shading and dashed lines indicating negative contours. Contour interval is (a) 20 and (b) 10 % $(\mathrm{g\ kg}^{-1})^{-1}$. Hatching indicates areas where the model could not be fitted.

negative and statistically significant over much of the globe—higher saturation specific humidity leads to a lower chance of a wet pentad. This could be due to the increased capacity of the air for holding moisture: warmer air has a higher saturation specific humidity, so that larger vertical motions are required to reach saturation. Hence, condensation (and therefore precipitation) is suppressed by high q_s due to the increased water-holding capacity of the air. The relationship is positive at high latitudes—higher saturation specific humidity increases the chance of a wet pentad. Figure 6b shows the q_s parameter estimates $(e^{\hat{\kappa}_2} - 1) \times 100\%$ for precipitation occurrence. There is a positive relationship over parts of Europe and the North Atlantic region but the most striking relationship is over the Tropics, particularly the Pacific Ocean. This relationship implies that increasing q_s might be responsible for increased precipitation in midlatitudes if there was more available water.

c. Dependence on the meridional temperature gradient

Figure 7a shows the NAO parameter estimates $(e^{\hat{\lambda}_3} - 1) \times 100\%$ for the occurrence of precipitation. Over much of the globe, there is not a strong statistically significant response. However, over the North Atlantic region, there is a positive response to the NAO, which shows that NAO positive behavior leads to increased chance of precipitation. There is some evidence of a tripole pattern with a nonlocal NAO response over the mid-Atlantic. Trigo et al. (2004) showed that there is a negative relationship between precipitation over the Iberian Peninsula and the NAO, which is consistent

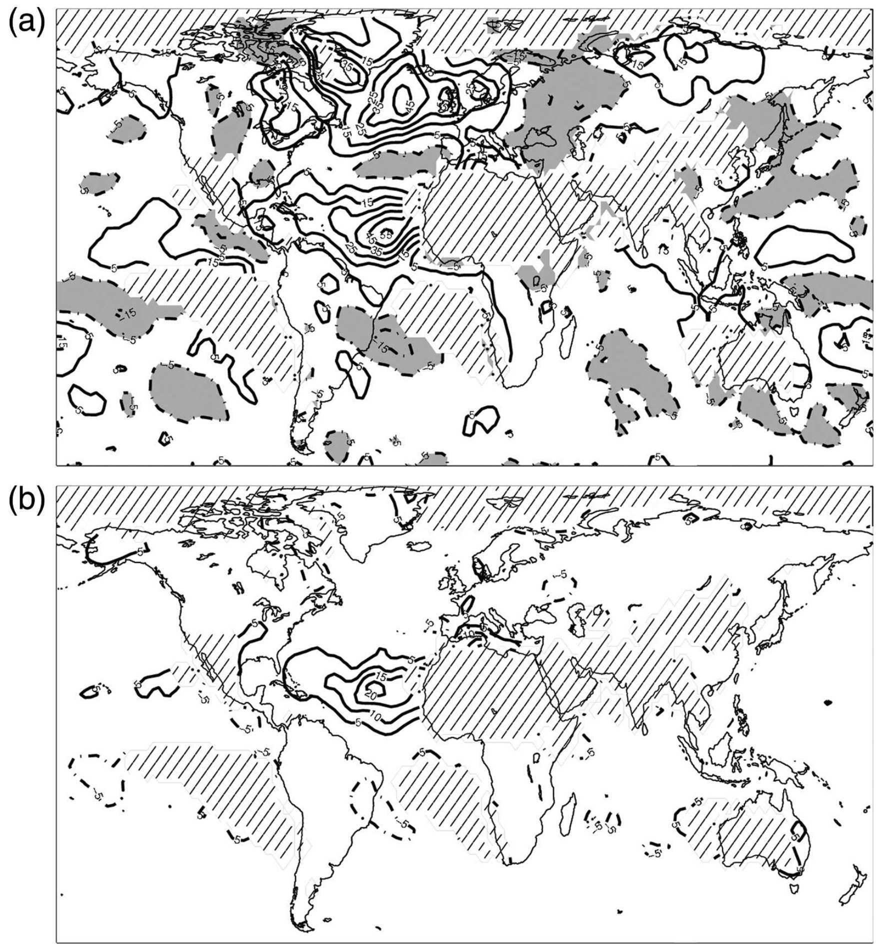

FIG. 7. NAO parameter estimates for October–March wet pentad GPCP precipitation (a) occurrence $(e^{\hat{\lambda}_3} - 1) \times 100\%$ and (b) amount $(e^{\hat{\kappa}_3} - 1) \times 100\%$ from the full model over the period 1979–2001 with the wet pentad threshold set to the 25th percentile. Units: %. The 1–2–1 smoothing is applied for readability. Solid lines indicate positive contours starting at 5% with dashed lines and shading to indicate negative contours starting at −5%. Contour interval is (a) 10% and (b) 5% and the zero line has been omitted. Hatching indicates areas where the model could not be fitted.

with the weak center of the dipole. The positive response over the mid-Atlantic is perhaps due to the enhanced easterlies associated with the NAO and the strengthening of the African easterly jet. Figure 7b shows the NAO parameter estimates $(e^{\hat{\kappa}_3} - 1) \times 100\%$ for the wet pentad precipitation amount. There is a large positive relationship over much of the Atlantic. The pattern observed here is similar to that in Fig. 7a over the mid-Atlantic with a positive relationship between the NAO and wet pentad occurrence. The tripole pattern is no longer visible, however, as the relationship in the North Atlantic is much weaker. Therefore, in addition to local SLP, NAO enhances both the occurrence and intensity of precipitation over much of the Atlantic region.

d. Residual time trends

The estimation of long-term trend in the data is difficult due to the short period available. It is also important to note that time trends can be due to interdecadal climate variability rather than secular climate change. Figures 8a,b show the time trend estimates in the odds of precipitation and the wet pentad precipitation amount from the models with only the annual cycle and the time trend but with the wet pentad threshold set to a constant 0.1 mm day^{-1}. Figures 8c,d show the same fields, but for a threshold defined by the 25th percentile. The fixed threshold of 0.1 mm day^{-1} represents the lowest physically plausible wet pentad threshold, and the 25th percentile represents a spatially variable

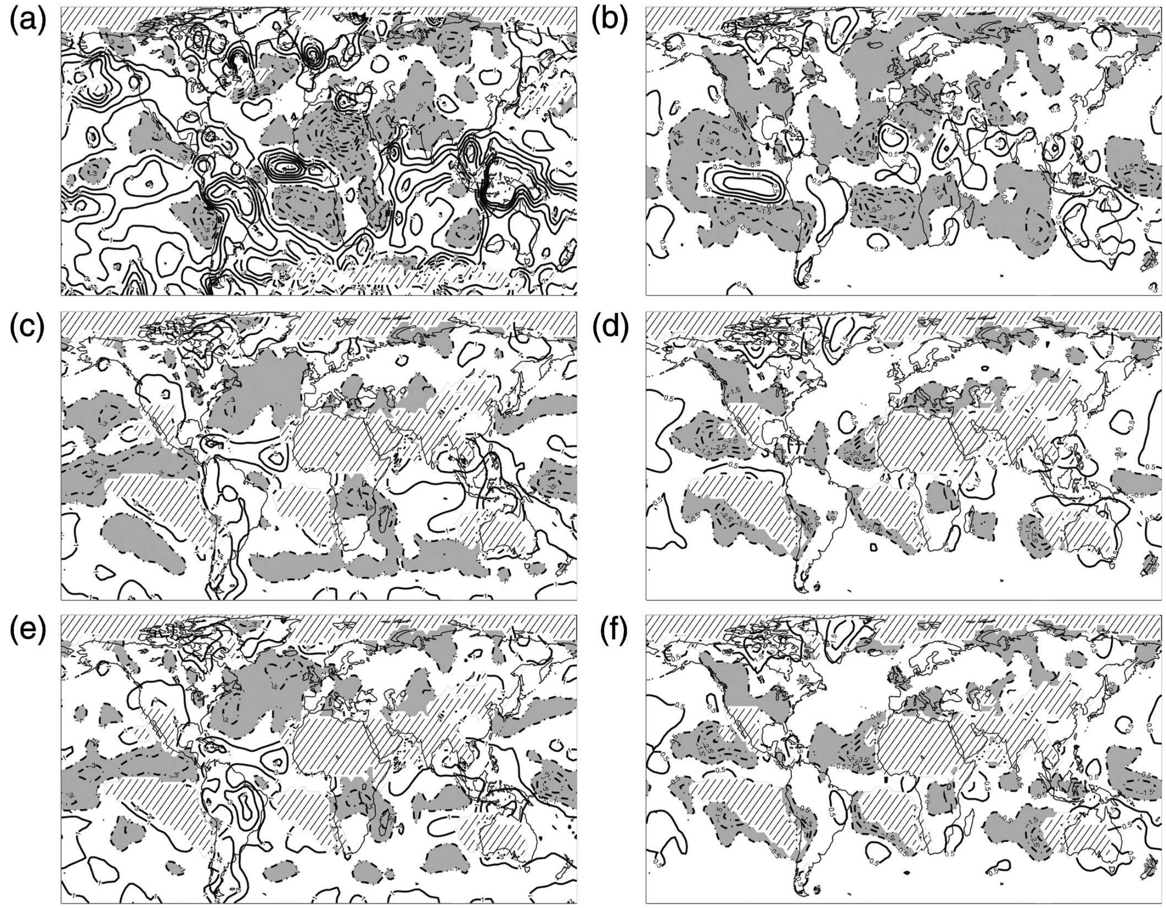

FIG. 8. Residual time trend estimates for October–March wet pentad GPCP precipitation (a) occurrence $(e^{\hat{\lambda}_4} - 1) \times 100\%$ and (b) amount $(e^{\hat{\kappa}_4} - 1) \times 100\%$ from the model without SLP, q_s, and the NAO with the wet pentad threshold set to 0.1 mm day^{-1}; (c) occurrence and (d) amount from the model without SLP, q_s, and the NAO with the wet pentad threshold set to the 25th percentile; (e) occurrence and (f) amount from the full model with the wet pentad threshold set to the 25th percentile. Units: % yr^{-1}. The 1–2–1 smoothing is applied for readability. Solid lines indicate positive contours starting at (a), (c), (e) 1 and (b), (d), (f) 0.5% yr^{-1}; dashed lines and shading to indicate negative contours starting at (a), (c), (e) -1 and (b), (d), (f) -0.5% yr^{-1}; zero line has been omitted and contour interval is (a), (c), (e) 2 and (b), (d), (f) 1% yr^{-1}. Hatching indicates areas where the model could not be fitted.

higher threshold. Comparison of Figs. 8a,c shows that the low fixed threshold gives positive trends over much of the globe, in contrast to the more negative trends for the higher variable threshold. The time trends in Fig. 8b are generally negative over the United Kingdom. Contrary to this, the trends obtained using a variable threshold in Fig. 8d are more positive. Decreases in dry pentad occurrence are compensated by increases of low-intensity wet pentad events (drizzle). The increase in low-intensity wet pentad events gives the impression that the mean of the wet pentad amounts is decreasing, whereas, in fact, larger-amplitude wet pentad amounts are increasing in intensity.

Figures 8e,f show time trend estimates in the odds of precipitation and the wet pentad precipitation amount from the models with all the explanatory variables included and with a wet pentad threshold defined by the 25th percentile. Comparison of Figs. 8e,f with 8c,d allows one to assess how much of the long-term time trend can be explained by the explanatory factors. The time trend is shown as the percentage change in the odds of a wet day $(e^{\hat{\kappa}_4} - 1) \times 100\%$. Therefore, a 5% increase in odds of 4:1 changes the odds to 4.2:1 (or 21:5), although the areas with time trends this large are unlikely to represent long-term trend. Figure 8c shows that there has been a decreasing trend in precipitation occurrence over the North Atlantic and over large parts of the Pacific Ocean. These patterns change slightly with the addition of the other explanatory variables (shown in Fig. 8e). The trend in precipitation occurrence is more negative over the North Atlantic and Europe and decreased the trends slightly over the North Pacific and the United States. Figure 8d shows the time trends in the wet pentad precipitation. There are generally small trends in midlatitudes, with slightly larger trends over tropical areas. There is a weak negative trend over midlatitude continental areas, with positive trends over midlatitude oceanic areas and the Tropics (particularly in the El Niño region). Folland et al. (2001) reported a general global increase since 1900, and Fig. 8d agrees with this as the time trends are generally positive. The time trends in the wet pentad amount change slightly with the inclusion of SLP, q_s, and the NAO (shown in Fig. 8f). Most interestingly, the trend over the North Atlantic region becomes more negative for the full model. This shows that SLP, q_s, and the NAO explain some but not all of the long-term trends in precipitation amounts.

5. Conclusions

It has been argued here that the vertical velocity of ascending air and saturation specific humidity are important multiplicative factors for large-scale, winter, extratropical precipitation. The quasigeostrophic ω equation was used to show that the midtropospheric meridional temperature gradient is also an important (yet often neglected) factor for large-scale vertical motion in the extratropics. It was also shown that these factors have a multiplicative effect on precipitation amount, and so statistical analyses of precipitation should respect this multiplicative property.

Local SLP, saturation specific humidity, and MTG are all physically motivated and statistically significant (at the 10% level) factors for accounting for variations in October–March pentad precipitation amounts. SLP was found to have a strong negative effect on both precipitation occurrence and the wet pentad amount over much of the globe, except in the Tropics, and on the poleward side of the storm tracks where the relationship was slightly positive. There was a generally negative effect of q_s on precipitation occurrence with exceptions over the tropical Pacific region, the deserts of North Africa and southern Asia, and around the Northern Hemisphere storm tracks, where there was a positive relationship. There was a positive effect of q_s on the wet pentad precipitation amount over the mid- and high latitudes and the tropical Pacific, and a negative relationship over the rest of the Tropics. The NAO, a proxy for the MTG, was found to be a statistically significant positive factor in addition to local SLP over the Atlantic Ocean for explaining both wet pentad occurrence and wet pentad amount. A drawback of using the NAO as a proxy for the meridional temperature gradient is that the meridional temperature gradient is only represented in the North Atlantic. In this study, this is an area of particular interest but similar proxies could be used to represent the meridional temperature gradient elsewhere, such as the Southern Annular Mode in the Southern Hemisphere. These results regarding the relationships between precipitation and some of the important explanatory factors might also be of further use in evaluation of model performance for climate modeling studies.

A negative long-term time trend was found in wet day occurrence in GPCP precipitation over 1979–2001 over the North Atlantic and parts of the Pacific Ocean with less coherent patchy trends over much of the globe. There was a generally increasing trend in wet day amount over the North Atlantic and much of the Pacific Ocean with decreases over Europe and North America. Saturation specific humidity and MTG are able to explain some but not all of the long-term linear time trends in precipitation. SLP trends fail to explain the increasing trends in precipitation amount over the North Atlantic region. The long-term time trends in precipitation are rather sensitive to the choice of threshold especially when the threshold is small. Time trends in the precipitation amount can be misleading when too low a threshold is applied. Increasing trends in low-intensity precipitation can lead to a spurious decreasing trend in wet-pentad precipitation totals. The problem in the low threshold model is most likely an artifact of the detection method, since many satellite techniques have difficulty in accurately representing low precipitation amounts. This problem is likely to be of reduced impact in more recent merged satellite records, such as those after 1987 after the introduction of Special Sensor Microwave Imager (SSM/I).

While the explanatory variables have been shown to account for some of the long-term time trend, they do not currently account for all of it. This suggests either that other factors are important (such as static stability), or that the long-term time trends in GPCP are inconsistent with other datasets. The estimation of long-term time trends is complicated by the relatively short period covered by GPCP, and the trends are not always consistent with longer, more localized, precipitation studies (such as over the United Kingdom; e.g., Jones and Conway 1997). Careful comparison of GPCP with longer regional or station-based datasets might be required to verify some of the trends over the short period. Another drawback of this approach is the sensitivity of time trends to the arbitrary choice of threshold. This might be addressed by the development of a method for estimating the wet pentad threshold based on goodness of fit of the Bernoulli and Gamma distributions to the data.

Acknowledgments. We wish to acknowledge Prof A. J. Thorpe and Prof B. J. Hoskins who both provided useful and insightful comments on some of this work. MRPS was supported by the Natural Environmental Research Council and a bursary from the Department of Meteorology, University of Reading.

REFERENCES

Barnston, A. G., and R. E. Livezey, 1987: Classification, seasonality and persistence of low-frequency atmospheric circulation patterns. *Mon. Wea. Rev.,* **115,** 1083–1126.

Brandsma, T., and T. A. Buishand, 1997: Statistical linkage of daily precipitation in Switzerland to atmospheric circulation and temperature. *J. Hydrometeor.,* **198** (1–4), 98–123.

Buishand, T. A., and A. M. G. K. Tank, 1996: Regression model for generating time series of daily precipitation amounts for climate change impact studies. *Stochastic Hydrol. Hydraul.,* **10** (2), 87–106.

——, and T. Brandsma, 1999: Dependence of precipitation on temperature at Florence and Livorno (Italy). *Climate Res.,* **12,** 53–63.

Chandler, R. E., and H. S. Wheater, 2002: Analysis of rainfall variability using generalized linear models: A case study from the west of Ireland. *Water Resour. Res.,* **38,** 1192, doi:10.1029/2001WR000906.

Coe, R., and R. D. Stern, 1982: Fitting models to daily rainfall data. *J. Appl. Meteor.,* **21,** 1024–1031.

DEFRA, 2001: To what degree can the October/November 2000 flood events be attributed to climate change? Department for Environment, Food and Rural Affairs Tech. Rep. FD2304 Final Rep., London, United Kingdom, 35 pp.

Durran, D. R., and L. W. Snellman, 1987: The diagnosis of synoptic-scale vertical motion in an operational environment. *Wea. Forecasting,* **2,** 17–31.

Eady, E. T., 1949: Long waves and cyclonic waves. *Tellus,* **1,** 35–52.

Folland, C., and Coauthors, 2001: Observed climate variability and change. *Climate Change 2001: The Scientific Basis,* J. T. Houghton et al., Eds., Cambridge University Press, 99–181.

Hawes, G., 2003: Property insurance in the UK—What does the future hold? *FloodRiskNet Newsletter,* Issue 2, Winter 2003, 9–10. [Available online at http://www.floodrisknet.org.uk.]

Hoskins, B. J., and M. A. Pedder, 1980: The diagnosis of middle latitude synoptic development. *Quart. J. Roy. Meteor. Soc.,* **106,** 707–719.

——, I. Draghici, and H. C. Davies, 1978: A new look at the ω-equation. *Quart. J. Roy. Meteor. Soc.,* **104,** 31–38.

Houghton, J. T., Y. Ding, D. J. Griggs, M. Noguer, P. J. van der Linden, and D. Xiaosu, Eds., 2001: *Climate Change 2001: The Scientific Basis*. Cambridge University Press, 944 pp.

Hurrell, J. W., 1995: Decadal trends in the North Atlantic Oscillation: Regional temperatures. *Science,* **269,** 676–679.

Jones, P. D., and D. Conway, 1997: Precipitation in the British Isles: An analysis of area-average data updated to 1995. *Int. J. Climatol.,* **17,** 427–438.

——, T. J. Osborn, and K. R. Briffa, 2003: Pressure-based measures of the North Atlantic Oscillation (NAO): A comparison and an assessment of changes in the strength of the NAO and its influence on surface climate parameters. *The North Atlantic Oscillation: Climatic Significance and Environmental Impact,* J. W. Hurrell et al., Eds., Amer. Geophys. Union, 51–62.

Madden, R. A., and J. Williams, 1978: The correlation between temperature and precipitation in the United States and Europe. *Mon. Wea. Rev.,* **106,** 142–147.

Murray, F. W., 1967: On the computation of saturation vapor pressure. *J. Appl. Meteor.,* **6,** 203–204.

Nelder, J. A., and R. W. M. Wedderburn, 1972: Generalized linear models. *J. Roy. Stat. Soc.,* **135A** (3), 370–384.

Pavan, V., N. Hall, P. Valdes, and M. Blackburn, 1999: The importance of moisture distribution for the growth and energetics of mid-latitude systems. *Ann. Geophys. Atmos. Space Sci.,* **17** (2), 242–256.

Peixoto, J. P., and A. H. Oort, 1992: *Physics of Climate.* American Institute of Physics, 520 pp.

Räisänen, J., 1995: Factors affecting synoptic-scale vertical motions: A statistical study using a generalized omega equation. *Mon. Wea. Rev.,* **123,** 2447–2460.

Rogers, R. R., and M. K. Yau, 1989: *A Short Course in Cloud Physics.* 3d ed. Pergamon, 290 pp.

Sanders, F., and B. J. Hoskins, 1990: An easy method for estimation of Q-vectors from weather maps. *Wea. Forecasting,* **5,** 346–353.

Sapiano, M. R. P., 2004: Trends and variability in observations of winter precipitation. Ph.D. thesis, University of Reading, Reading, United Kingdom, 165 pp.

Simmons, A. J., and J. K. Gibson, 2000: The ERA-40 Project Plan. ERA-40 Project Report Series 1, ECMWF, Reading, United Kingdom, 63 pp.

Stephenson, D. B., H. Wanner, S. Brönnimann, and J. Luterbacher, 2003: The history of scientific research on the North Atlantic Oscillation. *The North Atlantic Oscillation: Climatic Significance and Environmental Impact,* J. W. Hurrell et al., Eds., Amer. Geophys. Union, 37–50.

Stern, R. D., and R. Coe, 1984: A model fitting analysis of daily rainfall data. *J. Roy. Stat. Soc.,* **147A,** 1–34.

Trenberth, K. E., 1978: On the interpretation of the diagnostic quasi-geostrophic omega equation. *Mon. Wea. Rev.,* **106,** 131–137.

——, and D. J. Shea, 2005: Relationships between precipitation and surface pressure. *Geophys. Res. Lett.,* **32,** L14703, doi:10.1029/2005GL022760.

Trigo, R. M., D. Pozo-Vázquez, T. J. Osborn, Y. Castro-Díez, S. Gámiz-Fortis, and M. J. Esteban-Parra, 2004: North Atlantic Oscillation influence on precipitation, river flow and water resources in the Iberian Peninsula. *Int. J. Climatol.,* **24,** 925–944.

Türkeş, M., and E. Erlat, 2003: Precipitation changes and variability in Turkey linked to the North Atlantic Oscillation during the period 1930–2000. *Int. J. Climatol.,* **23,** 1771–1796.

Uvo, C. B., 2003: Analysis and regionalization of Northern European winter precipitation based on its relationship with the North Atlantic Oscillation. *Int. J. Climatol.,* **23,** 1185–1194.

Wanner, H., S. Bronnimann, C. Casty, D. Gyalistras, J. Luterbacher, C. Schmutz, D. B. Stephenson, and E. Xoplaki, 2001: North Atlantic Oscillation—Concepts and studies. *Surv. Geophys.,* **22** (4), 321–382.

Xie, P., J. E. Janowiak, P. A. Arkin, R. Adler, A. Gruber, R. Ferraro, G. J. Huffman, and S. Curtis, 2003: GPCP pentad precipitation analyses: An experimental dataset based on gauge observations and satellite estimates. *J. Climate,* **16,** 2197–2214.